ce/papers Proceedings in civil engineering

Ernst & Sohn A Wiley Brand

Check for updates

ORIGINAL ARTICLE

Crack Monitoring on Concrete Structures using Robust Distributed Fiber Optic Sensors

Max Herbers[1] | Bertram Richter[1] | Steffen Marx[1]

Correspondence

Max Herbers, M. Sc.
Technische Universität Dresden
Institute of Concrete Structures
August-Bebel-Str. 30/30a
01062 Dresden
Email: max.herbers@tu-dresden.de

[1] Institute of Concrete Structures, Technische Universität Dresden, Dresden, Germany

Abstract

The possibility to measure strains continuously using distributed fiber optic sensors (DFOS) offers enormous potential for structural health monitoring. Cracks can be automatically detected, localized and crack widths calculated. To address the relevant questions of choosing the right DFOS and appropriate application technique for monitoring existing structures, two 4 m long reinforced concrete beams were loaded under service loads in a 4-point bending test. The DFOS were either bonded directly to the smooth concrete surface or along a groove. For comparison, another DFOS was integrated into the specimen. It is demonstrated that with the used adhesive, a good strain transfer from the specimen to the DFOS can be ensured even with subsequent installation. In order to detect all cracks with high reliability, robust DFOS with a monolithic cross section should be preferred for the practical use. The accuracy of crack width measurement was verified through reference measurement via digital image correlation. For the monolithic DFOS, all measurement deviations were within the tolerance range of ±0.05 mm. With layered sensing cables, significant misinterpretations occurred due to strongly damped strain curves.

Keywords

Distributed fiber optic sensing, Crack monitoring, Robust DFOS, Monolithic and multilayered DFOS, Application method, Subsequent installation

1 Introduction

The aging infrastructure poses challenges for Germany, as well as many other European countries. Most bridges were built during the 1960s and 1970s [1] and are therefore slowly reaching the end of their service life. Demolishing the old bridges and rebuilding is not expedient from both ecological and economic perspectives. In order to ensure mobility, it will be crucial to maintain existing structures in the upcoming decades. Measured in terms of bridge area, approximately 69% of bridges on federal highways in Germany were built in prestressed concrete and 17% in reinforced or plain concrete [1]. Thus, concrete structures play a significant role in the German bridge stock.

Cracking is a major contributor to damages on concrete bridges, with spalling and exposed reinforcement being additional damage patterns that are favored by the presence of cracks [2]. Today, crack pattern and crack width are usually recorded manually in a time-consuming process. In the future, the crack monitoring can be largely automated by using distributed fiber optic sensors (DFOS), which can lead to a more efficient use of limited personnel resources in structural inspections.

Due its wide range of applications, the use of DFOS will be crucial in the future of structural health monitoring (SHM), both for existing and new structures to be built. Continuous strain measurement enables to capture diverse information on the structure's condition. One specific application is crack monitoring, where the integration of DFOS into the structure or subsequently installed on the existing structures can automatically detect and locate cracks, as well as calculate crack widths.

Fiber optic measurement technology is already used for various experimental investigations in laboratories [3–5]. By integrating DFOS into concrete, it becomes possible to gain insights into the material and bond behavior [6–8]. Even at low load levels, this technology allows for highly accurate strain measurement [9].

In the past, there has been a major research effort in the field of crack monitoring on concrete structures [10–12]. BERROCAL et al. [13] for example, used thin polyamide coated optical fibers that were bonded directly to the surface of a rebar and proposed a method for crack width calculation on the basis of distributed steel strain measurements. Both the crack locations and the crack widths could be determined with high accuracy. Filigree polyam-

ide coated fibers are a relevant option for use in the laboratory, but are not a reliable solution for practical applications due to their low robustness.

FISCHER et al. [14] compared the strain curves of both filigree and robust DFOS during investigations on reinforced concrete beams. The thin polyimide-coated DFOS glued to the concrete surface in the tension zone did not provide reliable strain values due to the stiff bond which probably caused a fiber breakage. Plausible strain values were exhibited by a robust, multilayer DFOS (V9) and a DFOS with an additional nylon buffer, with the latter one showing significantly more pronounced strain peaks.

The layered V9 was also used for crack monitoring in further experiments [15; 16], whereby the cracks could mostly be detected, and the crack widths measured with high accuracy. However, in some cases, especially for closely spaced cracks, single cracks were not detected, leading to misinterpretations as shown later.

While first practical applications of crack monitoring have been undertaken on tunnel shells [17; 18] and bridges [19–22], further research is required to determine the appropriate DFOS type and application method for the given measurement task. In this study, the signal quality of robust DFOS with a multilayer and monolithic cross section is compared and evaluated in terms of reliability for crack monitoring. Additionally, the influence of the application technique is being investigated to identify subsequent DFOS installation techniques providing a reliable monitoring of existing structures.

2 Crack monitoring using DFOS

2.1 Fiber optic measurement technique

One of the main features of DFOS is the ability to measure strains due to temperature changes or mechanical effects along the fiber length. During the measurements, light is sent into the optical fiber. A small portion of the light is backscattered due to local defects and variations in the refractive index, see Figure 1. At the beginning of a measurement, the so-called fingerprint of the DFOS must be determined. This is a fluctuating intensity profile of the backscattering along the fiber that remains stable under constant external conditions. Due to strains resulting from temperature changes and/or mechanical stresses, with the elongation of the fiber also frequency of the backscattered light shifts. To achieve continuous measurement, the DFOS is divided into small gauges (< 5 mm). Strains can be determined by analyzing local frequency shifts in the single gauges [23; 24].

For fiber optic measurements, three different types of light backscattering occurring within an optical fiber can be utilized namely RAYLEIGH, BRILLOUIN, and RAMAN scattering [25]. BRILLOUIN and RAYLEIGH scattering are sensitive to thermal and mechanical strain changes, allowing the use for distributed temperature sensing (DTS) and distributed strain sensing (DSS). As it is indistinguishable, whether strains are due to mechanical or thermal influences, compensation of thermal influences are necessary for mechanical strain measurements under varying temperatures and vice versa [26].

Devises utilizing BRILLOUIN scattering enable measurements across extended ranges of several kilometers, with the disadvantage of relatively low spatial resolution. As a result, BRILLOUIN scattering is primarily employed for monitoring long linear structures, such as roads, dams, or tunnels. In contrast, devices using RAYLEIGH scattering currently support a maximum measurement length of up to 70 m for DSS [24], but with much finer spatial resolution (as low as 0.65 mm), making it the preferred solution for crack monitoring.

In construction industry, RAMAN scattering is mainly used to measure temperature profiles over longer distances with a spatial resolution of up to 50 cm. Therefore, it can be used for the temperature compensation for BRILLOUIN and RAYLEIGH measurements.

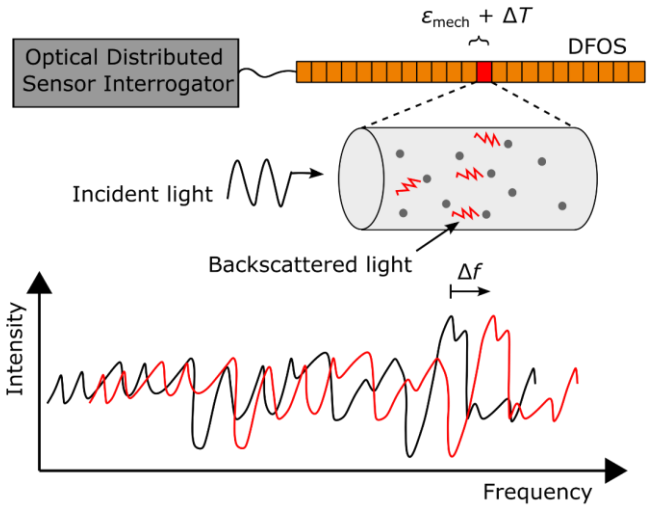

Figure 1 Evaluation of the RAYLEIGH backscattering over individual gauges along the optical fiber

2.2 DFOS choice and bond behavior

Although there has been progress in SHM using DFOS and field applications have been demonstrated, accurate calculation of crack widths for reinforced concrete structures is still challenging. The choice of DFOS type and application technique strongly influences the reliability and accuracy of crack monitoring. The bond behavior between the glass core and the host material, such as the concrete surface, is crucial for crack detection and localization. The stiffness of the composite is determined by the layered DFOS structure (glass core, cladding, coating and, if required for additional mechanical protection, buffer and jacket), as well as the application technique, including the type of adhesive and surface preparation.

To enable reliable detection and localization of closely spaced cracks, the bond between the DFOS and host material must be sufficiently stiff. However, a certain level of flexibility is also necessary to prevent DFOS breakage in the crack area, where high local strains occur, see Figure 2. The stiffness of the coating and adhesive determines the quality of strain transfer and the transfer length l_t, with stiffer coatings and adhesives resulting in shorter transfer lengths but also a higher risk of breakage. To ensure both reliable crack detection and prevention of breakage in the area of relevant crack widths, the DFOS-adhesive stiffness should be carefully selected.

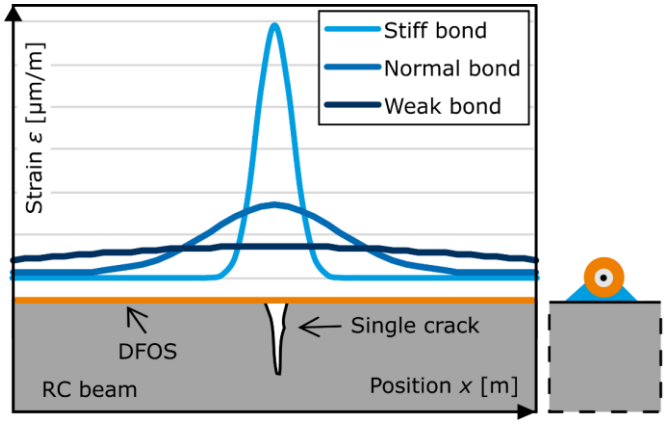

Figure 2 Strain distribution in the area of a single crack for different bond stiffnesses (left) and multilayer structure of a DFOS consisting of coating, cladding and glass core (right) [27]

Several analytical and also numerical models [28–32] exist in the literature that describe the strain transfer between the DFOS and the host material (e.g., concrete or reinforcement). However, for crack monitoring, it is not the "real" concrete strain that is of most interest, but rather the ability to detect each individual crack through strain peaks. In cases where the bond is too weak, two closely spaced cracks can be smeared within a single strain peak, leading to significant misinterpretations. As will be shown later, if all cracks are detected, the influence of the overall stiffness (DFOS type and application technique) on the calculated crack width is small.

There are various types of DFOS available for measuring concrete strain. However, choosing the right DFOS is not trivial and depends on a multitude of factors, such as robustness, stiffness, maximum compressive or tensile strains, and durability [33]. Depending on the specific use case, very filigree DFOS with a diameter of less than 0.2 mm as well as robust DFOS with an additional protective jacket to prevent mechanical damage can be employed [27].

2.3 Crack width calculation

The characteristic crack widths w_{cr} in reinforced concrete structures are determined in accordance with the regulations by multiplying the difference between the mean strains of concrete ε_{cm} and steel ε_{sm} by the maximum crack spacing $s_{r,max}$:

$$w_{cr} = (\varepsilon_{sm} - \varepsilon_{cm})\, s_{r,max} \qquad (1)$$

Although steel strains can be measured with DFOS, they cannot measure the "real" concrete strains as the concrete embedded DFOS bridges the crack, resulting in large strain peaks in this area. In reality, the actual concrete strains drop to zero in the direct vicinity of the crack and increase again with increasing distance from the crack because part of the stresses are reintroduced by bond into the concrete.

Approaches for calculating crack widths based on DFOS attached to the reinforcement or embedded into the concrete can be found in the literature [12–14]. Due to the lower installation effort as well as the more pronounced strain peaks, crack monitoring with DFOS embedded in concrete or subsequently applied to the surface is recommended. This enables the detection of even the smallest strain peaks and thus the onset of crack formation. The finest cracks can be detected before they become visible to the human eye [34].

Both calculation methods are based on the assumption that the crack width results from the integral of the DFOS strain distribution ε^{DFOS}. For DFOS bonded to concrete, the measured strains are composed of the crack opening and a small part of elastic concrete strains. Hence, the effect of tension stiffening (TS) ε^{TS} must be compensated for:

$$w_{cr,i} = \int_{l_{t,i}^{-}}^{l_{t,i}^{+}} \varepsilon^{DFOS}(x) - \varepsilon^{TS}(x)\, dx \qquad (2)$$

To define the integration range, the half crack spacing to the adjacent crack on the right l_t^+ and left l_t^- is chosen as the transfer length l_t . Since concrete strains are not directly measured, for TS, it is assumed that it reaches its maximum of 100 µm/m between the cracks at the integration boundaries, decreasing linearly to zero as the distance to the crack decreases. The schematic approach is shown in Figure 3. As a first approximation, it is acceptable to neglect the effect of TS, as it is small.

Further background information on crack width calculation using steel and concrete embedded DFOS and a sensitivity analysis of the different influencing parameters can be found in [35]. The authors provide an open source Python framework that enables a semi-automated calculation of crack widths.

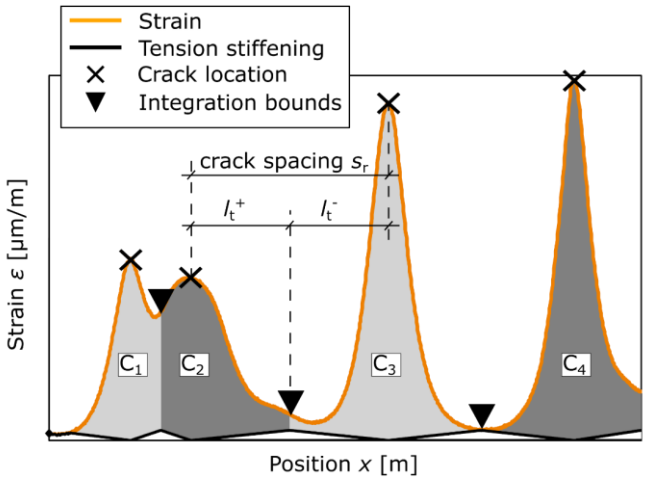

Figure 3 Crack width calculation method for concrete embedded DFOS

3 Experimental investigations

The objective of the laboratory experiments was to identify suitable DFOS fulfilling three key requirements: a) accurately detect, b) localize, and c) measure the width of cracks within the range of the SLS in concrete structures. Two different DFOS were used for the measurements, which have a certain robustness due to their structure and can therefore withstand the harsh site conditions. Additionally, the study investigated the influence of the application methods on the quality of the strain curves and consequently of the crack monitoring. DFOS were either embedded in the concrete, installed in a groove or directly

glued to the concrete surface. It must be clarified whether reliable crack monitoring is also possible with DFOS that have been installed subsequently. To answer these questions, two reinforced concrete beams were loaded in a 4-point bending test under service load level.

3.1 Specimen and materials

The 4 m long specimens have a rectangular cross section with $b \times h$ = 30 cm × 40 cm and a concrete cover of 20 mm, see Figure 4. As there were no shear forces V present, stirrups were omitted in the center of the field to avoid affecting the crack pattern.

For concreting, a flowable concrete (consistency class F5) with a mean concrete compressive strength f_c of 42.7 N/mm² and a maximum aggregate diameter of 8 mm was used. The YOUNGS'S modulus E_c was determined to 30300 N/mm². A detailed overview of the material parameters can be found in [27]. To reduce moisture evaporation, polyethylene sheets were placed over the specimens after concreting. The beams remained in the same indoor climate (with a temperature of 21.0 °C ±2.0°C and relative humidity of about 40%) until loading, with the formwork removed five days after concreting. Despite post-treatment measures, shrinkage cracks occurred in the area of the stirrups.

3.2 Test setup

The specimens were loaded 29 days after concreting, using hydraulic jacks to prestress them against each other at the ends and steel cylinders to keep them apart, as depicted in Figure 5. This loading configuration is equivalent to a 4-point bending test, with the tensile zones located on the outer sides of the specimens to facilitate DIC-based crack monitoring. To minimize friction between the specimens and the concrete foundation, a special multi-layer bedding was used. After reaching a target load of 50 kN per press, hexagon nuts were fixed at the load cells to maintain a constant deflection throughout the 112-day testing period, during which the constraint force, concrete and steel strains, and crack width development were monitored. This contribution focuses on the results obtained during and immediately after the load application. The effects resulting from the viscous concrete behavior as well as the long-term behavior of the DFOS will be published subsequently.

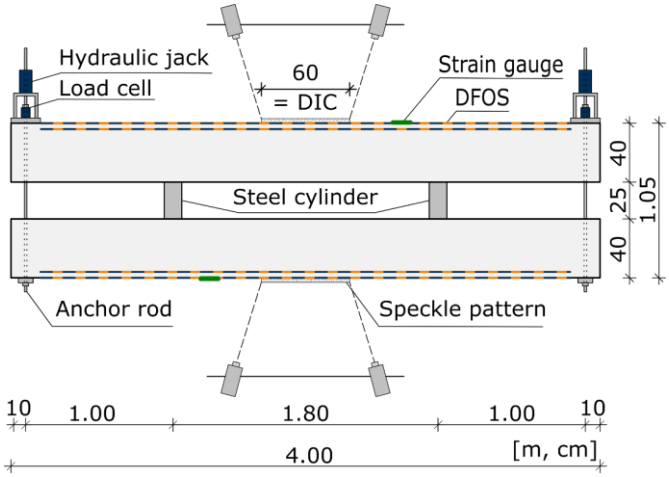

Figure 5 Test setup in top view and sensor layout

3.3 Strain measurements

As illustrated in Figure 4 and Figure 5, the concrete strains on the outer surface and at the level of the longitudinal reinforcement in the tension zone were recorded using different measurement techniques.

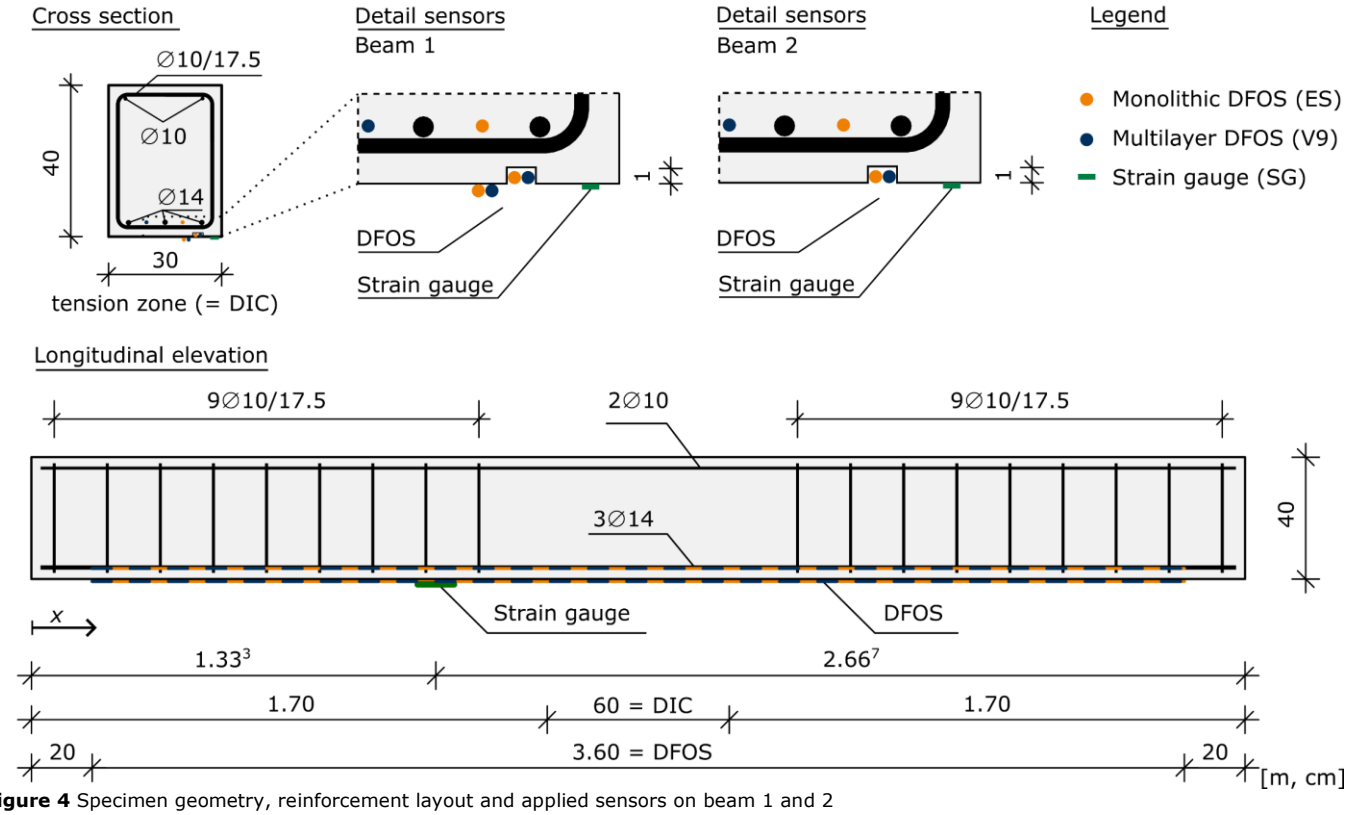

Figure 4 Specimen geometry, reinforcement layout and applied sensors on beam 1 and 2

Within the experiments, both very filigree DFOS with a diameter of less than 0.2 mm and construction site-compatible, robust DFOS such as the V9 or the EpsilonSensor (ES) were compared. The results of the different filigree DFOS are primarily of interest for laboratory testing and can be found in [27]. This contribution focuses on the use of robust DFOS as shown in Figure 6. The V9 (∅ = 3.2 mm) has a layered cross section consisting of a polyamide (PA) buffer and a metal tube to protect the internal single-mode (SM) fiber. The ES, on the other hand, has a monolithic cross section with a diameter of 3.0 mm. In a pultrusion process, the SM fiber is integrated into polyester (PE) fibers, which are impregnated with a special epoxy resin [22]. Both DFOS have a structured surface to ensure proper mechanical interlocking with the concrete.

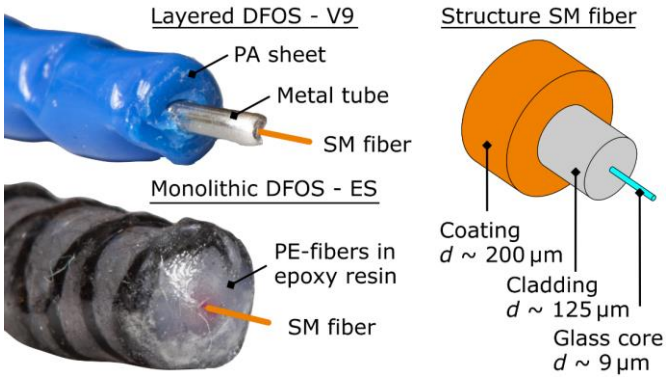

Figure 6 Comparison of the cross section design of robust DFOS (graphic: Max Herbers, photos: Stefan Gröschel)

Of particular interest was the subsequent DFOS installation. Before gluing, the concrete surface and also the groove were cleaned with air pressure of dust and coarse dirt. At first, the DFOS were fixed in position with an epoxy adhesive at several points along the sensor length. The DFOS were then glued along the whole length with a 2-component injection mortar with a short processing time, which also allows overhead installation on existing structures.

The optical distributed sensor interrogator (ODiSI) 6100 was used as a data acquisition unit. In order to be able to detect microcracks as well, the highest spatial resolution available was used with a distance of 0.65 mm between measuring points. For practical monitoring applications, a larger gauge length can be chosen due to the debonding effect between the concrete and the DFOS, leading to a smeared strain peak. During loading only two DFOS applied in the groove of beam 1 were measured with a sample rate of 1 Hz. After reaching the target load level, the remaining DFOS were each measured for about 30 s. Since frequency shift in fiber optic measurements results from both temperature changes and mechanical effects, temperature compensation is essential for SHM. However, since the tests were carried out under nearly constant climatic conditions, compensation was not necessary in the context of this study.

In addition, the crack propagation in the tensile zone in the center of the field over a length of 600 mm was captured via digital image correlation (DIC). The commercial system GOM ARAMIS® with a stereo camera system with 12 megapixels resolution was used. To measure local strains at the concrete surface, a strain gauge (SG) was placed at x = 1.333 m on the outer surface of each beam.

4 Results and discussion

4.1 Strain development during loading

The strain development during loading is presented in Figure 7 for three different load levels: $0.5F_{cr}$, $1.0F_{cr}$ and $2.0F_{cr}$, where the concrete cracking force F_{cr} was calculated with the characteristic concrete tensile strength $f_{ctk} = 0.7f_{ctm}$. The diagrams show the measured raw data without post-processing for the DFOS glued in the groove of beam 1.

The strain curves are compared with the theoretical strain distribution according to the theory of elasticity. The strains in the tensile zone of the uncracked beam can be calculated using the following formula:

$$\varepsilon_c(x) = \frac{M_y(x)}{E_c I_y} z \qquad (3)$$

where $M_y(x)$ is the in-plane bending moment, z is the distance to the neutral axis, I_y is the ideal moment of inertia considering the different material stiffnesses, E_c is the modulus of elasticity of the concrete.

At low loading ($F = 0.5F_{cr}$), both DFOS show good agreement with the SG as well as the theoretical strain curves. Despite the low loading far below the cracking force F_{cr}, first peaks appear in the strain curves indicating the formation of single cracks. These very small cracks can be attributed to pre-damage of the concrete structure in the area of the stirrups. Despite the measures after concreting, first shrinkage cracks could already be identified. In the shear force-free areas, where no stirrups were present, an almost constant strain curve is observed, which indicates an intact concrete matrix. At this very low strain level, the measurement noise of approximately ±10 µm/m is evident. The noise depends on the choice of the gage pitch and increases with increasing measurement resolution [36]. If necessary, part of the noise can be smoothed during post processing.

When the cracking force ($F = 1.0F_{cr}$) is reached, further cracks appear in the center of the field, which can be detected by both DFOS types. However, compared to the V9, the ES shows much more pronounced strain peaks, which ensures that even the smallest cracks in the crack formation stage can be detected by the monolithic DFOS. Due to the stiff bond within the cross section as well as between the DFOS and the concrete, the strains between the cracks decrease significantly. The V9 shows a much more damped strain curve.

With further load increase ($F = 2.0F_{cr}$), these differences become more significant. While for the ES strain peaks of more than 3500 µm/m can be observed, the maxima for the V9 are not even half as large. Between the cracks, the measured strains of the V9 are also significantly higher than the theoretical maximum strain that can result from the TS of the concrete ($\varepsilon_{ct} \approx 100$ µm/m). Despite the clearly different strain curves, the average strain and thus the calculated elongation of the beam is approximately the same.

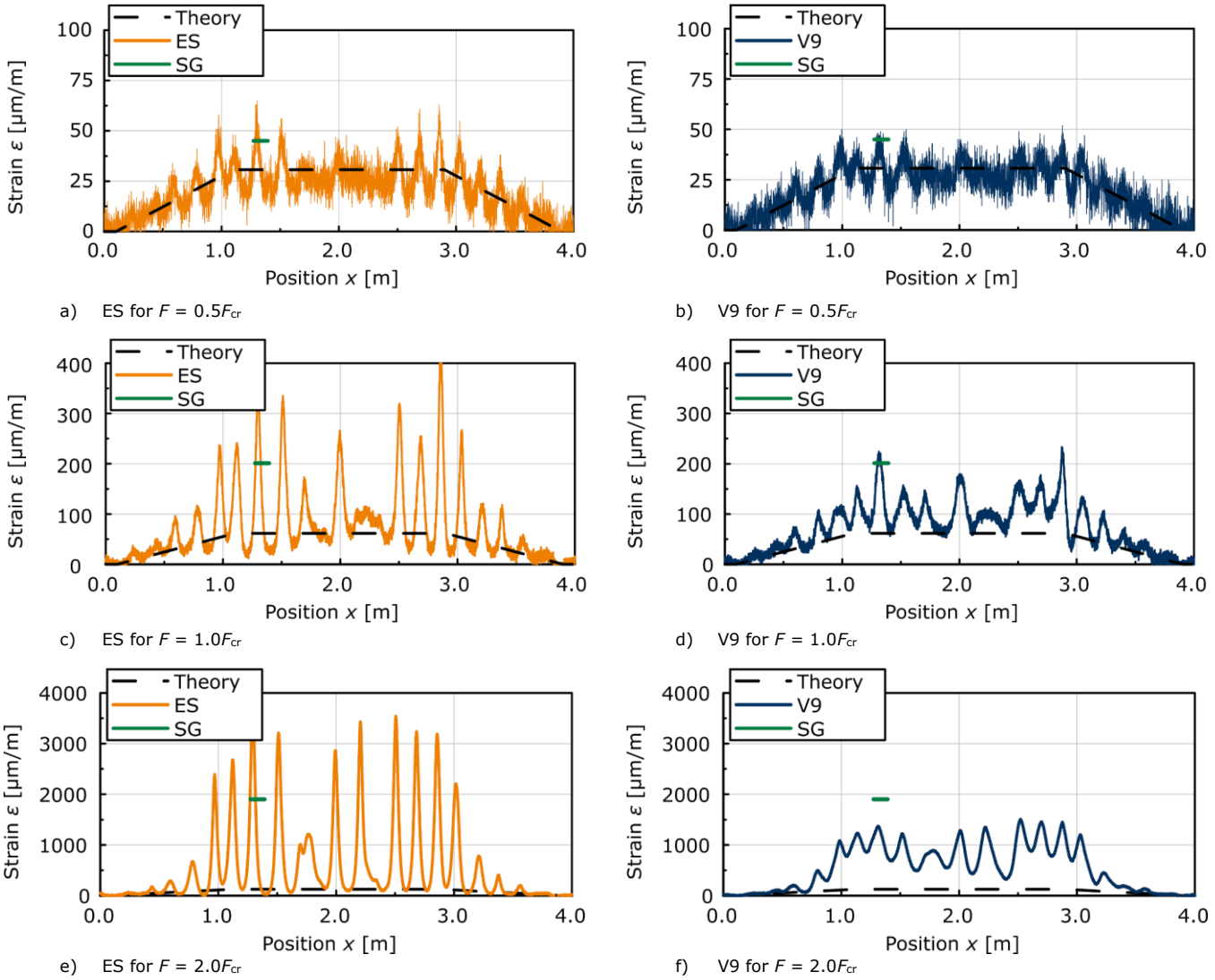

Figure 7 Strain development along the length for beam 1 at different load levels (DFOS installed in groove)

It is assumed that the attenuated strain curves of the V9 can be attributed to the multi-layer DFOS design (see Figure 6). As the load increases, slippage occurs between the layers, causing a strain redistribution from the highly stressed to the less stressed areas. On the other hand, ES shows proper strain transfer across the cross section due to its monolithic structure. Combined with the low axial stiffness, pronounced strain peaks occur in the area of the cracks, which enables a high reliability for crack detection.

4.2 Influence of the subsequent installation

DFOS can be integrated into formwork of newly built structures to monitor them from the beginning of their lifespan. However, for existing structures, the only option is to subsequently mount the DFOS to the component. DFOS can be either glued directly onto the concrete surface or embedded in a groove. Since the DFOS can only measure changes in crack width for existing structures, an initial measurement must be taken using a crack width ruler or crack magnifier to determine the absolute crack width.

To ensure that the subsequent installation does not affect the reliability of the crack monitoring, it is necessary to determine its impact. It must be guaranteed that the DFOS bonded to the smooth concrete surface or in the groove have a sufficiently rigid bond with the specimens; otherwise, single closely spaced cracks might remain undetected.

As an example for beam 1, the strain curves after reaching the target load are shown for different application techniques in Figure 8. The V9 embedded in the specimen is no longer available for comparison of the application method, as it was damaged either during concreting or subsequent transport. The influences are discussed separately for both DFOS in the following.

4.2.1 Monolithic DFOS (ES)

In Figure 8 a) it can be seen that for all three DFOS along the examined length of 1.0 m at the center of the field, six pronounced strain peaks occur. The strain peaks coincide with the visually perceived number of cracks. This indicates that cracks can be detected irrespective of the method of installation. However, there are differences in the strain curves. Despite bonding to the smooth concrete surface, this DFOS exhibits the most pronounced strain peaks, indicating adequate bonding between the sensor and the specimen. To a small extent, the higher strains are due to the greater distance from the neutral fiber. For this reason, the DFOS embedded in the specimen should have lower strain peaks than the one glued into the groove. However, this is not the case. Possibly due to the

adhesive's short processing time which may have caused incomplete embedding of the DFOS within the adhesive's matrix in certain areas. In addition, during installation, the DFOS was first placed in the groove and then the high-viscosity adhesive was filled in. This may have prevented the bond on the underside of the DFOS from being fully formed. As a result, the DFOS in the groove shows a slightly attenuated strain curve.

4.2.2 *Layered DFOS (V9)*

Unlike the monolithic DFOS ES, both V9 DFOS show only five strain peaks within the considered length. The closely spaced cracks detected with the ES at $x \approx 1.75$ m are smeared with the V9 as one wider peak. There is no clear trend in the height of the minima and maxima, as they occur at about the same level. The strains measured by the DFOS on the surface occasionally exceed those recorded by the groove DFOS, and vice versa. As with the ES, it is possible that the V9 was not fully embedded in the adhesive at some points.

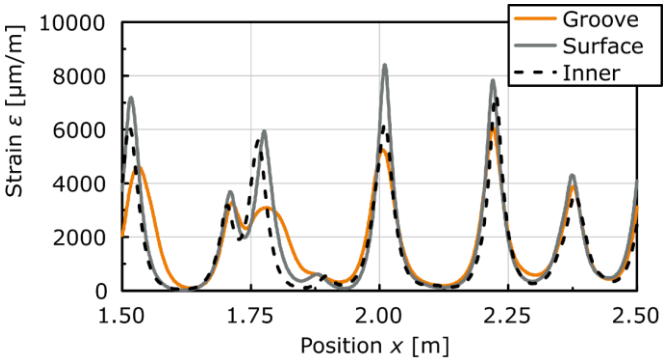

a) Strain curves for ES

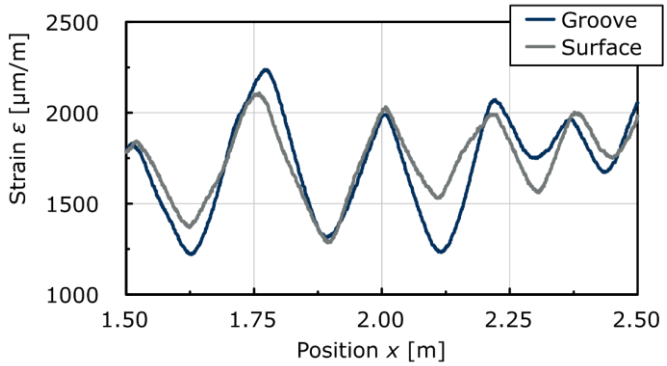

b) Strain curves for V9

Figure 8 Influence of the installation method for beam 1 DFOS

4.2.3 *Conclusions on installation technique*

No significant differences were observed in the strain curves among the various installation methods. Even with a subsequent installation, a good bond could be achieved between the component and the DFOS using the 2C adhesive, even if the DFOS were directly glued to the smooth concrete surface. Extensive surface preparation (such as exposing the aggregate) was not necessary. However, for the sake of robustness, e.g., against mechanical impact and fire, as well as to enhance durability, groove installation is recommended for long-term monitoring of existing structures. To ensure a reliable bond between the DFOS and the component, the groove should be chosen sufficiently large to allow the DFOS to be fully embedded in the adhesive matrix. Before gluing, the groove must be cleaned of dust and coarse impurities.

4.3 Crack width calculation

In the following, the crack widths calculated from fiber optic measurements are compared with those of DIC measurements. Figure 9 a) illustrates the crack pattern and strain distribution of beam 1 over a measuring length of 60 cm for DIC. Here, four cracks (C_1 to C_4) with crack widths from 0.17 mm to 0.34 mm, and a smaller crack, labelled as "micro-crack" (M_1), with a width of 0.03 mm at the same height as the DFOS were recorded. Thus, there is a broad spectrum of crack widths that can be utilized for the verification of the DFOS measurements.

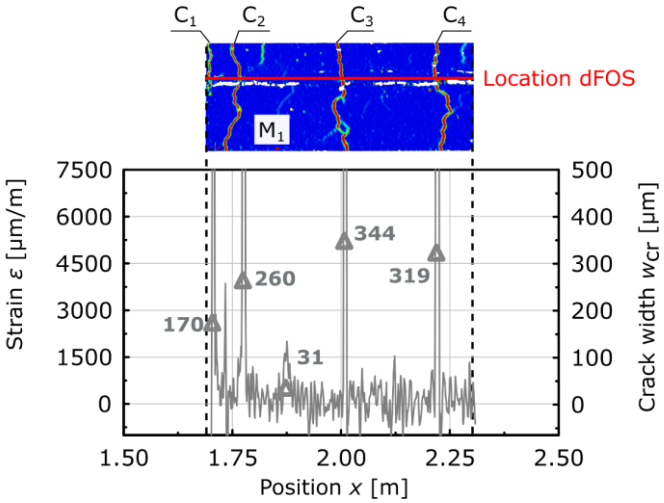

a) Crack pattern, strains and crack widths from DIC

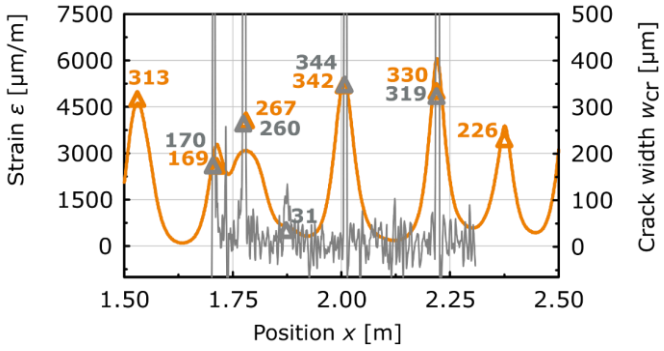

b) Comparison of DIC and ES

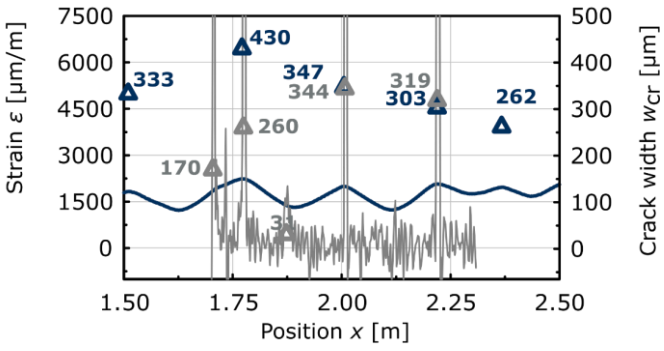

c) Comparison of DIC and V9

Figure 9 Strain curves and crack widths for DIC and DFOS inside groove of beam 1 (cf. [27])

The DIC measurement shows that strains approach infinity in the area of the cracks (absence of concrete) and decrease strongly between the cracks. Note that despite the

relatively small measuring volume the noise is much higher than for the DFOS. The subfigures 9 b) and c) present the strain curves and crack widths for different DFOS on beam 1, which were installed in the groove. The crack widths for the DFOS were calculated, following the method described in Section 2.3, using the half crack spacing as the transfer length l_t and considering TS with a maximum strain of 100 µm/m. For automated crack detection, a peak finding algorithm is used. To define whether a peak is a crack, the term prominence is introduced, which describes how far a peak stands out from its surrounding [35]. Due to the low noise level, the prominence for automated crack detection could be set to 100 µm/m.

As shown in Figure 9 b), proper strain transfer was observed for the ES, with all cracks except for the microcrack detected. The presence of pronounced strain peaks enables precise localization of cracks. The crack locations and also the calculated crack widths show good agreement with the DIC measurement. Figure 9 c) shows the much smoother strain curve of DFOS V9, where the strain peaks of the closely adjacent cracks C_1 and C_2 are smeared into one peak, and consequently, the two cracks are interpreted as one, leading to a significant overestimation of the crack width ($w_{cr,DFOS}$ = 0.43 mm ›› 0.26 mm resp. 0.17 mm). It should be noted that the sum of the two single cracks corresponds to the calculated DFOS-crack width of 0.43 mm. In regions where single cracks are detected via strain peaks as such, the calculated crack widths are in good agreement with DIC.

4.4 Verification of crack widths

Finally, as shown in Figure 10, the accuracy of the crack width calculation is verified using DIC as a reference measurement. Due to practical relevance, only cracks with a width of more than 0.10 mm were considered. Thus, there were four cracks available for comparison for each beam. In subfigures a) to c), the crack widths obtained from the DFOS measurement are plotted against the DIC crack widths for the three different application methods. If the calculated crack width lies on the bisector, the two measuring techniques for crack width determination agree completely. The dotted line indicates the tolerance range of ±0.05 mm, which is assumed to be the maximum permissible deviation for practical use.

Figure 10 a) shows the results for the DFOS bonded to the smooth concrete surface of beam 1 ("B1"). For the ES, there is an almost perfect agreement with the DIC, which is also evident in the comparison of the mean crack widths: $w_{cr,ES}$ = 0.277 mm ≈ $w_{cr,DIC}$ = 0.273 mm. As previously illustrated (cf. Figure 9), only three cracks could be detected along the measuring length of 60 cm with the V9. Due to the fact that two cracks are smeared into one peak, the crack width is significantly overestimated. The mean crack width for the V9 is $w_{cr,V9}$ = 0.370 mm and is therefore much higher than the DIC measurement.

As shown in Figure 10 b), for the DFOS measurements in the groove, an ES and a V9 were available for beam 1 and 2, respectively. A similarly positive result was obtained for the ES as in the previous analysis, where the DFOS were directly bonded to the surface. Despite more pronounced strain peaks for DFOS glued to the surface, the area under the strain curve remains approximately the same. Therefore, the crack widths for the ES in the groove also agrees well with the reference measurement. Only for beam 2 ("B2"), the crack widths are slightly underestimated in three cases, but the deviations between DFOS and DIC are within the tolerance range. Also with the V9 in the groove, the smoothed strain profile largely overestimates the crack widths in two cases. In two other cases, where the individual cracks were detected as such, the measured crack widths are also outside the tolerance range (overestimation of crack widths).

As the cracks close towards the neutral axis, it is consistent with the observation in Figure 10 c) that the DFOS crack widths measured at the level of the rebars are smaller than the crack widths detected with DIC on the surface. The crack widths for the ES are mostly between the bisector and the lower limit for the allowable deviation. The mean crack width for ES is 0.042 mm lower than the DIC crack width. In contrast, the crack widths of the V9 fluctuate around the reference measurement. As before, two cracks were also smeared into one. The V9 installed in beam 1 has failed, as mentioned earlier.

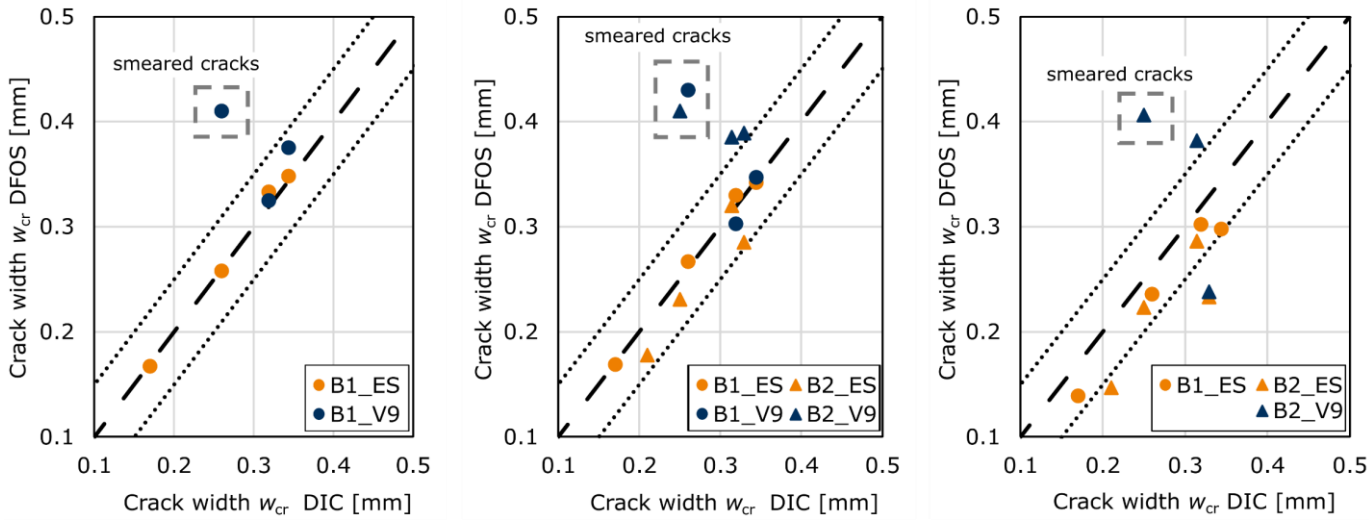

a) DFOS on surface b) DFOS in groove c) DFOS inside the beams

Figure 10 Calculated crack widths compared to DIC depending on DFOS installation

In summary, it can be stated that the influence of the application technique for the investigated robust DFOS on the crack width calculation is small. Reliable crack width determination is possible even for DFOS subsequently installed on existing structures. For the monolithic ES, maximum deviation from DIC was 0.044 mm and thus within the defined tolerance range of ±0.05 mm. The layered V9 showed significantly longer transfer lengths than the ES. Especially with small crack spacings, there is a risk that for two cracks only one strain peak is formed, resulting in a substantial overestimation of the actual crack width. In this paper, the use of robust DFOS with a diameter ∅ ≥ 3 mm was investigated. For crack monitoring in laboratory tests, more filigree DFOS, e.g., with an acrylate or ORMOCER® coating, may also be suitable [27].

5 Conclusions

In the past, several studies have demonstrated the general feasibility of crack width measurement using DFOS. In order to ensure reliable crack monitoring on existing structures, in the present study, the influence of application technique as well as the choice of the DFOS type on the signal quality was investigated. Two different robust DFOS, suitable for harsh construction site conditions, were compared. Therefore, two 4 m long reinforced concrete beams were loaded in a 4-point bending test under service load level.

For subsequent installation, a stiff and homogeneous bond between the DFOS and the component over the entire measuring length must be ensured, as otherwise smeared strain curves may occur. The tests have shown that also for subsequently installed DFOS, a proper strain transfer can be achieved with the 2-component adhesive used. For DFOS bonded directly to the smooth concrete surface, even the most pronounced strain peaks were visible. Bonding in a groove involves the risk that the DFOS is not fully embedded in the adhesive matrix. Nevertheless, to increase robustness and ensure long-term measurement, installation along a groove is recommended. The groove size should be chosen sufficiently large to ensure that the DFOS can be fully embedded in the adhesive matrix.

It was demonstrated that the choice of DFOS has a significant impact on the measurement quality. The advantages of monolithic over layered DFOS are in the stiffer strain transfer between the host material and the optical fiber. While layered DFOS result in attenuated strain curves due to possible slippage between individual layers, DFOS with a monolithic cross section exhibit distinct strain peaks, allowing even very small cracks (<0.05 mm) to be detected, precisely located and their crack widths calculated accurately. For all monolithic DFOS subsequently installed, the deviations for the calculated crack widths were within the tolerance range of ±0.05 mm. The average absolute deviation for the ES laid within a groove on beam 1 and 2 was ±0.015 mm, which indicates a perfect suitability for crack monitoring. The damped strain curves of layered DFOS can cause two closely spaced cracks be blurred within a single strain peak, resulting in a significant overestimation of crack widths.

It was shown that the potential of crack monitoring using DFOS can also be exploited for existing structures, where the DFOS has to be installed subsequently. In the future, the efficiency of structural inspection is expected to be strongly increased with the use of fiber optic sensing. Thereby, the presented crack monitoring is just one example of the numerous potential application fields.

Acknowledgements

This paper presents some of the results of the research project IDA-KI (Automated assessment of monitoring data for infrastructure constructions using AI and IoT) funded by the Federal Ministry for Digital and Transport, Germany, within the innovation program mFUND (funding reference: 19FS2013A). We would like to thank the funding authority for their financial support as well as the research partners for the productive cooperation within the project.

References

[1] Bundesanstalt für Straßenwesen (2021) *Brückenstatistik* [online]. https://www.bast.de/DE/Statistik/Bruecken/Brueckenstatistik.html [Zugriff am: 10. Jan. 2022].

[2] Schnellenbach-Held, M.; Peeters, M.; Miedzinski G. (2015) *Intelligente Brücke - Schädigungsrelevante Einwirkungen und Schädigungspotenziale von Brückenbauwerken aus Beton* – BASt-Bericht B 110. Essen.

[3] Becks, H. et al. (2023) *Monitoring concept for the propagation of compressive fatigue in externally prestressed concrete beams using digital image correlation and fiber optic sensors*. Fatigue & Fracture of Engineering Materials & Structures 46, H. 2, S. 514–526.

[4] Becks, H. et al. (2022) *Application of fiber optic measurement in textile-reinforced concrete testing.* Structural Concrete 23, H. 4, S. 2600–2614.

[5] Ungermann, J. et al. (2022) *Eccentric punching tests on column bases – New insights into the inner concrete strain development.* Engineering Structures 262.

[6] Zdanowicz, K. et al. (2022) *Distributed fiber optic sensors for measuring strains of concrete, steel, and textile reinforcement: Possible fields of application.* Structural Concrete.

[7] Koschemann, M.; Curbach, M.; Marx, S. (2022) *Investigation of local bond behavior using distributed optical fiber sensing*. Hofmann, J.; Plizzari, G. [Eds.] Bond in Concrete. Stuttgart. Stuttgart: Universität Stuttgart, pp. 133–145.

[8] Speck, K. et al. (2021) *Dehnungsmessung bei mehraxialen Druckversuchen an Beton mittels faseroptischer Sensoren*. Beton- und Stahlbetonbau 116, H. 3, S. 212–221.

[9] Clauß, F.; Ahrens, M. A.; Mark, P. (2021) *A comparative evaluation of strain measurement techniques in reinforced concrete structures–A discussion of assembly, application, and accuracy*. Structural Concrete

22, H. 5, S. 2992–3007.

[10] Tan, X.; Bao, Y. (2021) *Measuring crack width using a distributed fiber optic sensor based on optical frequency domain reflectometry*. Measurement 172.

[11] Henault, J.-M. et al. (2012) *Quantitative strain measurement and crack detection in RC structures using a truly distributed fiber optic sensing system*. Construction and Building Materials 37, S. 916–923.

[12] Brault, A.; Hoult, N. (2019) *Monitoring Reinforced Concrete Serviceability Performance Using Fiber Optic Sensors*. ACI Structural Journal 116, H. 1.

[13] Berrocal, C. G.; Fernandez, I.; Rempling, R. (2020) *Crack monitoring in reinforced concrete beams by distributed optical fiber sensors*. Structure and Infrastructure Engineering 17, H. 1, S. 124–139.

[14] *Fischer, O.; Thoma, S.; Crepaz, S. (2019) Distributed fiber optic sensing for crack detection in concrete structures*. Civil Engineering Design 1, 3-4, pp. 97–105.

[15] Fernandez, I.; Berrocal, C. G.; Rempling, R. (2021) *Long-Term Performance of Distributed Optical Fiber Sensors Embedded in Reinforced Concrete Beams under Sustained Deflection and Cyclic Loading*. Sensors (Basel, Switzerland) 21, Nr. 19.

[16] Berrocal, C. G. et al. (2021) *Assessment and visualization of performance indicators of reinforced concrete beams by distributed optical fibre sensing*. Structural Health Monitoring 20, H. 6, S. 3309–3326.

[17] Vorwagner, A. et al. (2021) *Verteilte Rissbreitenmessung im Betonbau mittels faseroptischer Sensorik – Neue Anwendung von verteilten faseroptischen Messsystemen*. Beton- und Stahlbetonbau 116, H. 10, S. 727–740.

[18] Gómez, J.; Casas, J. R.; Villalba, S. (2020) *Structural Health Monitoring with Distributed Optical Fiber Sensors of tunnel lining affected by nearby construction activity*. Automation in Construction 117.

[19] Barrias, A. et al. (2018) *Application of distributed optical fiber sensors for the health monitoring of two real structures in Barcelona*. Structure and Infrastructure Engineering 14, H. 7, S. 967–985.

[20] Novák, B. et al. (2021) *Einsatz kontinuierlicher faseroptischer Sensoren zum Monitoring von Bestandsbrücken*. Beton- und Stahlbetonbau 116, H. 10, S. 718–726.

[21] Bednarski, Ł. et al. (2022) *The Smart Nervous System for Cracked Concrete Structures: Theory, Design, Research, and Field Proof of Monolithic DFOS-Based Sensors*. Sensors 22, Nr. 22.

[22] Howiacki, T. et al. (2023) *Crack Shape Coefficient: Comparison between Different DFOS Tools Embedded for Crack Monitoring in Concrete*. Sensors 23, H. 2, S. 566.

[23] Samiec, D. (2011) *Verteilte faseroptische Temperatur- und Dehnungsmessung mit sehr hoher Ortsauflösung*. Photonik, H. 6, S. 34–37.

[24] Bado, M. F.; Casas, J. R. (2021) *A Review of Recent Distributed Optical Fiber Sensors Applications for Civil Engineering Structural Health Monitoring*. Sensors 21, Nr. 5.

[25] Bao, X.; Chen, L. (2012) *Recent progress in distributed fiber optic sensors*. Sensors 12, Nr. 7.

[26] Clauß, F.; Ahrens, M. A.; Mark, P. (2022) *Thermo-mechanical experiments on reinforced concrete beams: Assessing thermal, mechanical, and mixed impacts on fiber optic measurements*. Structural Concrete 23, Nr. 6, pp. 3521–3537.

[27] Herbers, M. et al. (2023) *Crack Monitoring on Concrete Structures – Comparison of Various Distributed Fiber Optic Sensors with Digital Image Correlation Method*. Structural Concrete (accepted for publication).

[28] Alj, I. et al. (2020) *Experimental and Numerical Investigation on the Strain Response of Distributed Optical Fiber Sensors Bonded to Concrete: Influence of the Adhesive Stiffness on Crack Monitoring Performance*. Sensors 20, Nr. 18.

[29] Her, S.-C.; Huang, C.-Y. (2016) *The Effects of Adhesive and Bonding Length on the Strain Transfer of Optical Fiber Sensors*. Applied Sciences 6, H. 1, S. 13.

[30] Bassil, A. et al. (2020) *Concrete Crack Monitoring Using a Novel Strain Transfer Model for Distributed Fiber Optics Sensors*. Sensors 20, Nr. 8.

[31] Feng, X. et al. (2013) *Theoretical and experimental investigations into crack detection with BOTDR-distributed fiber optic sensors*. J. Eng. Mech., H. 139, S. 1797–1807.

[32] Zhang, S. et al. (2021) *A mechanical model to interpret distributed fiber optic strain measurement at displacement discontinuities*. Structural Health Monitoring 20, Nr. 5, pp. 2584–2603.

[33] Alj, I. et al. (2021) *Environmental Durability of an Optical Fiber Cable Intended for Distributed Strain Measurements in Concrete Structures*. Sensors 22, Nr. 1.

[34] Sieńko, R. et al. (2018) *Strain and crack analysis within concrete members using distributed fibre optic sensors*. Structural Health Monitoring 18, 5-6, S. 1510–1526.

[35] Richter, B.; Herbers, M.; Marx, S. (2023) *Crack Monitoring on Concrete Structures with Distributed Fiber Optic Sensors – Towards Automated Data Evaluation and Assessment*. Structural Concrete (under review).

[36] Luna Innovations Inc. (2020) *Optical Distributed Sensor Interrogator Model ODiSI 6 – User's Guide ODiSI 6*. Blacksburg, VA, USA.